3D Segmentation of the Prostate via Poisson Inverse Gradient Initialization

Bing Li, Abhay V. Patil, John A. Hossack and Scott T. Acton
University of Virginia, Charlottesville, VA 22904, USA

ABSTRACT

Accurate segmentation and volumetric assessment of the enlarged prostate is critical to assessment of cancer progression. Moreover, 3D segmentation is necessary for treatment in both radiotherapy and brachytherapy. We propose a 3D segmentation solution for ultrasound images of the prostate based on deformable surfaces. The deformable surfaces are propelled by the vector field convolution (VFC) external force model. This external force has both computational efficiency and solution quality advantages over existing techniques such as gradient vector flow (GVF). A salient aspect of the segmentation solution proposed here is the ability to automatically initialize the deformable surface in 3D. The initialization method exploits a novel Poisson inverse gradient technique that essentially solves the inverse problem from the external force field to the external energy and determines the most likely coarse segmentation. We validate our 3D segmentation on simulated images of the prostate. Furthermore, simulated data show that PIG initialization leads to a 60% reduction in segmentation error for high curvature contours.

Index Terms— Deformable surfaces, prostate cancer, vector field convolution, Poisson inverse gradient.

1. INTRODUCTION

The American Cancer Society estimated that there would be approximately 27,900 prostate cancer related deaths and approximately 234,000 new cases diagnosed in 2006. Currently prostate cancer screening is based on Prostate Specific Antigen (PSA) blood testing, free PSA testing and Digital Rectal Examination (DRE). While the sensitivity of these techniques, in combination, is generally considered acceptable for clinical screening, the specificity and Positive Predictive Value (PPV) are considerably less than ideal. When the PSA is used, there exists a significant gray area (4 - 10 ng/mL) in which cancers may be missed or that a negative biopsy is requested. Consequently, there is significant interest in high quality diagnostic imaging of the prostate. Ultrasound is the preferred modality of the grounds of low cost (capital and operating), adequate spatial resolution and real-time image acquisition. In particular, there is a clinical need to accurately track the volumetric size of a prostate cancer as it evolves over time or regresses due to treatment. This motivates the need to rapid and accurate segmentation of the prostate and of cancer lesions within prostate images.

Deformable models [1], have been widely used for image segmentation and object tracking. The most widely used deformable models include *active contours*, a.k.a. *snakes* [2], and *deformable surfaces* [1]. Given an initialization, the deformable model is morphed on the image domain in order to capture a desired image segment. The computational process by which this deformation is achieved is typically the result of minimizing an energy functional subject to certain constraints. Such an energy functional usually contains two terms: an internal energy, which constrains the smoothness and tautness of the model, and an external energy, which attracts the elastic model to the *features of interest* (FOI). The solution to the energy minimization problem can be formulated as a force balance equation, where the internal force generated from the internal energy equilibrates the external force calculated from the external energy. There are several different types of static external forces documented in the literature [3-5].

Although extensive research has been completed to improve the deformable model performance, the subject of deformable model initialization has received considerably less attention. The initialization is a critical factor in the ultimate solution quality of the deformable model. The most popular and convenient way is to initialize the deformable models is by employing some naïve geometric model such as a circle in 2D or sphere in 3D. The major drawback of this simple initialization approach is that the deformable model may need a large number of iterations to converge or may converge to clutter away from the desired target. An alternative is manual initialization via manual selection of initial points. Even though manual initialization is effective, manually drawing a complex 3D surface, for example, is extremely a difficult and error-prone process. Two examples of manual initialization processes are provided by [6, 7].

The main contribution of this paper is to provide a new method to automatically initialize deformable models by estimating the underlying external energy via solution of the Poisson equation. The idea is to select an initial model with an associated energy that approaches the minimum energy. This novel method accelerates the convergence of deformable models via initializing the deformable model close to the FOI. This paper is organized as follows. We review the basis of deformable surfaces in Section 2, and introduce and demonstrate our method, *Poisson inverse gradient* (PIG) initialization, in Section 3. All equations are given for 3D images, from which the analogous 2D equations can be formulated. At last, we draw conclusions in Section 4.

2. DEFORMABLE SURFACES

A deformable surface is defined by mapping a bivariate parameter domain $(m,n)\in[0,1]^2$ into $\mathbb{R}^3$, where a surface point is given by $\mathbf{v}(m,n)=\left[x(m,n),\, y(m,n),\, z(m,n)\right]$. The surface is deformed by minimizing

$$\varepsilon=\int_0^1\int_0^1\left\{\frac{\alpha}{2}\sum_{a=m,n}\left\|\frac{\partial\mathbf{v}}{\partial a}\right\|^2+\frac{\beta}{2}\sum_{a,b=m,n}\left\|\frac{\partial^2\mathbf{v}}{\partial a\partial b}\right\|^2+E_{\text{ext}}(\mathbf{v})\right\}dmdn\,, \quad (1)$$

where α and β are weighting parameters constraining the degree of the smoothness and tautness of the surface, respectively, and $E_{\text{ext}}:\mathbb{R}^3\to\mathbb{R}$ denotes the external energy, the value of which is small at the FOI, such as edges [1-3].

At the minima of (1), the surface must satisfy the Euler-Lagrange equation

$$\alpha\Delta_{m,n}\mathbf{v}-\beta\Delta_{m,n}^2\mathbf{v}-\nabla E_{\text{ext}}=0\,, \quad (2)$$

where $\Delta_{m,n}\mathbf{v}=\frac{\partial^2\mathbf{v}}{\partial m^2}+\frac{\partial^2\mathbf{v}}{\partial n^2}$ is the Laplacian operator. This equation can be considered as a force balance equation

$$\mathbf{f}_{\text{int}}(\mathbf{v})+\mathbf{f}_{\text{ext}}(\mathbf{v})=0 \quad (3)$$

where $\mathbf{f}_{\text{int}}(\mathbf{v})=\alpha\Delta_{m,n}\mathbf{v}-\beta\Delta_{m,n}^2\mathbf{v}$ is the internal force to constraint the smoothness and tautness of the surface, and

$$\mathbf{f}_{\text{ext}}(\mathbf{v})=-\nabla E_{\text{ext}}(\mathbf{v}) \quad (4)$$

is the standard external force that draws the surface toward the FOI. If the *edge map* is defined as $e=-E_{\text{ext}}$, then $\mathbf{f}_{\text{ext}}=\nabla e$, i.e., the standard external force is the gradient of the edge map.

A number of research groups have generalized (3) via replacing the standard external force with the sum of other forces generated from the image and/or the contour [3, 4, 8]. In addition to the standard external force (4), there are several attractive candidates for the external force, including the *distance force*, *gradient vector flow* (GVF), and *vector field convolution* (VFC). The distance force points to the closest edge by taking the negative gradient of the distance transformation of the edge points [3]. In this case, the edge points are extracted from the edge detector. The GVF field is calculated as a diffusion of the standard external force [4]. And third, the VFC field is computed by convolving the edge map *f* with a predefined vector field kernel [5], which is chosen in this paper for its superior noise robustness and lower computational cost.

Recall that the external force is defined as the negative gradient of the external energy in (4). Then, for a given external force field **f**, there should exist an external energy *E* such that the negative gradient of *E* is **f**. Unfortunately, **f** is not conservative in general, i.e., **f** may not be the negative gradient of any scalar function. In the next section, we introduce a method to approximate *E* by solving the Poisson equation, which is used for initializing deformable models.

3. AUTOMATIC MODEL INITIALIZATION

3.1. Poisson inverse gradient

The first step of the initialization approach is to estimate the external energy *E* given the external force **f**, from which the initial model is extracted. Let Ω be a subset of $\mathbb{R}^3$ with boundary ∂Ω. Let $E:\mathbb{R}^3\to\mathbb{R}$ be an unknown scalar function and $\mathbf{f}:\mathbb{R}^3\to\mathbb{R}^3$ be a known vector field defined over Ω. The *Poisson inverse gradient* (PIG) approach estimates the optimal external energy *E* such that the negative gradient of *E* is the closest vector field to **f** in the L_2-norm sense,

$$E=\arg\min_E\int_\Omega\left|-\nabla E-\mathbf{f}\right|^2. \quad (5)$$

To minimize (5), *E* must satisfy the Poisson equation

$$\Delta E=-\operatorname{div}\mathbf{f}\,, \quad (6)$$

where $\operatorname{div}\mathbf{f}=\partial u/\partial x+\partial v/\partial y+\partial w/\partial z$ is the divergence of $\mathbf{f}=[u,v,w]$. In order to solve (6) for deformable models, the Dirichlet boundary conditions [9]

$$E\big|_{\partial\Omega}=E_{\text{ext}}\big|_{\partial\Omega}=-e\big|_{\partial\Omega}\,, \quad (7)$$

is specified to maintain fidelity with respect to the edge map *e*, which is used to generate the vector field **f**.

Thus, the solution to our initialization problem of segmenting the prostate is a Poisson equation solution. And the numerical solution to Poisson equation is well studied [9]. To be specific, on a discrete grid [1, M_x] × [1, M_y] × [1, M_z], the region Ω is define as a set of pixels. For each pixel *p* in Ω, let N_p denote the set of its 6-connected neighbors. The boundary ∂Ω is now defined as $\partial\Omega=\{p\notin\Omega: N_p\cap\Omega\neq\varnothing\}$. Let $\mathbf{f}_p$ denote the value of **f** at *p*. By approximating the Laplacian and the divergence operators, (6) and (7) can be rewritten as the discrete Poisson equation: for all $p\in\Omega$,

$$\sum_{q\in\Omega\cap N_p}E_q-\left|N_p\right|E_p=\sum_{q\in\partial\Omega\cap N_p}e_q+\operatorname{div}\mathbf{f}_p \quad (8)$$

where the number of neighbors $\left|N_p\right|$ may less than 6 depending on if *p* is on the image border.

In our applications, the region is defined as

$$\Omega=\{p: e_p\le\tau\}\,, \quad (9)$$

where τ is a threshold. All the pixels in the edge map *e* that have a value larger than τ are preserved and used as boundary condition since they represent the FOI, whereas other pixels will be estimated. If Ω is consisted of several separated regions, each region can be calculated separately to reduce the system complexity.

Equation (8) is a symmetric positive-definite banded sparse system, which can be solved in numerous ways, including successive over-relaxation (SOR), conjugate gradient (CG) techniques, fast Fourier transform (FFT) techniques and multigrid methods. The computational complexity comparison is shown in Table 1. For prostate

segmentation in our cancer research, we implemented the PIG on a Dell Dimension 9150 computer with Pentium D 2.8 GHz CPU, 1GB RAM, and MATLAB 7.0. It takes 0.4 s to solve a 20,000 pixels system. A multigrid implementation in C will provide a faster solution for larger regions [10].

In order to calculate the PIG of 3D external forces with limited computational resources, subsampling is usually necessary (with current PC implementations). The 3D image, or volume, can be subsampled to a lower resolution without distorting the FOI, which can significantly reduce the system size. If the system is still too large to be computed, the volume can be divided into several sub-volumes, which are calculated separately.

Fig. 1(a) demonstrates an ultrasound image of prostate. In order to eliminate the multiplicative ultrasound noise, termed *speckle*, speckle reducing anisotropic diffusion (SRAD) is employed to preprocess the image [11]. The edge map and the VFC external force are calculated from the processed image. After threshold the edge map using (9) and apply area close morphological filter to eliminate small features, the region Ω is obtained. The PIG result overlapped with the isolines provides a different view of the external force fields, a.k.a. the underlying external energy, as demonstrated in Fig. 1(b). An *isoline* is a curve connection points where the PIG result has the same value, and this value is termed *isovalue*. By observing Fig. 1(c), we find that the isolines close to the FOI can be used as a good initialization for active contours, because they provide excellent shape approximations and have low external energy that is close to the minimum external energy.

3.2. Poisson inverse gradient initialization

After calculating the PIG result of the external force, a high-quality initial deformable model can be achieved by selecting an isoline or isosurface with proper isovalue. Analog to the isolines in 2D, *isosurfaces* in 3D are surfaces that pass through the isovalues of the PIG result. The marching cubes algorithm is employed to render the isosurface in our applications [12]. Under the assumption that the target FOI is the global minimum, the isoline or isosurface with minimum external energy is chosen as the initialization given a set of predefined isovalues. Note that there may be more than one isoline or isosurface correspond to a given isovalue, only the longest isoline or the largest isosurface is chosen as the optimal initial model because it has the lowest energy. In our prostate cancer application, contours and surfaces are represented by connected discrete vertices. Therefore, given the isovalue λ_k, the size of the *l*-th isoline/isosurface is estimated by the number of vertices n_k^l, and the corresponding model energy ε_k^l is calculated by

$$\varepsilon_k^l = n_k^l \left(\lambda_k - E_{\max} \right), \tag{10}$$

and the minimum model energy is

$$\varepsilon_k = \min_l \varepsilon_k^l = \left(\lambda_k - E_{\max} \right) \max_l n_k^l, \tag{11}$$

where $E_{\max} = \max_{x,y,z} E(x,y,z)$ is the maximum external energy, which assures the model energy ε_k is negative.

The automatic PIG initialization procedure for prostate segmentation is implemented in the following steps:

a) Calculate the PIG result *E* of the external force **f**.
b) Define *K* isovalues $\{\lambda_k, k = 1,2,...,K\}$.
c) For each isovalue λ_k, calculate the model energy ε_k of the largest isoline/isosurface using (11).
d) The largest isoline/isosurface of isovalue λ_{k^*} yielding the minimum model energy is chosen to be the optimal initial model, i.e., $k^* = \arg\min_k \varepsilon_k$.

Furthermore, other constraints may be applied to the isoline/isosurface selection to refine the initialization, such as the selected isoline/isosurface must be close. Fig. 1(d) shows that a snake is initialized by the optimal close isoline and successfully captures the prostate boundary in 205 iterations.

Note that the PIG result of distance forces is the negative distance transform of the edge map, which provides a shortcut for deformable model initialization. If the PIG of a 3D external force field is precluded by computational expense, the isosurface of the negative distance transform of the edge map can be used as the initial deformable surface.

4. RESULTS

This initialization method can accommodate broken edges, which is exemplified in Fig. 2. If the maximum distance between edge fragments is *d*, the selected isovalues have to be larger than *d*/2. Otherwise, the isolines might pass through the gap between fragments. As shown in Fig. 2(c), with this high quality initialization, the VFC snake successfully captures the broken edges in only 5 iterations, which is a very difficult, if not impossible, task for VFC snakes if initialized as simple geometric objects.

We also generate several geometric shapes of increasing curvature (from a tube shape of zero curvature to a "C" shape with high curvature) to evaluate the impact of PIG initialization on segmentation accuracy. The accuracy is measured using the normalized area error, which is computed by the normalized difference between the area of the segmentation and the area of the ground truth segment. The PIG initialization method is compared with simple rectangular initialization. As shown in Fig. 3, the PIG method reduces the error given by the simple initialization method by 60% for high curvature contours. The contrast is also dramatic in computational cost – the average number of iteration needed to converge is 12 for the PIG method, as compared to 94 for the rectangular initialization.

Finally, this automatic initialization method is applied to a simulated 3D ultrasound image of prostate lesion [13]. As shown in Fig. 4(a-b), since the selected isosurface is close to the FOI, the VFC deformable surface converges in only 20 iterations. In contrast, the deformable surface

requires over 100 iterations to converge if initialized as a small sphere at the center. Note that these 100 surface updates also necessitate complicated surface remeshing. The center slice of the original 3D image overlapped with the intersection of the initial and final deformable surface are demonstrated in Fig. 4 (c).

5. CONCLUSIONS

In this paper, we introduced a new method termed the Poisson inverse gradient (PIG) initialization to estimate the underlying external energy from the given external force, and automatically initialize high-quality curves/surfaces for active models. The deformation procedure can be significantly accelerated by a properly selected initialization. We proposed two methods (subsampling and subdivision) to reduce the size of the system. This initialization approach can accommodate broken edges, and be employed for prostate segmentation. The design of an optimally efficient implementation of PIG is an open research problem.

ACKNOWLEDGEMENTS

This work was made possible in part by the financial support of DoD CDMRP grant W81XWH-01-1-0240.

REFERENCES

[1] D. Terzopoulos, A. Witkin, and M. Kass, "Constraints on deformable models - recovering 3D shape and nonrigid motion," *Artificial Intelligence*, vol. 36, pp. 91-123, 1988.

[2] M. Kass, A. Witkin, and D. Terzopoulos, "Snakes - active contour models," *International J. of Computer Vision*, vol. 1, pp. 321-331, 1987.

[3] L. D. Cohen and I. Cohen, "Finite-element methods for active contour models and balloons for 2-D and 3-D images," *Pattern Analysis and Machine Intelligence, IEEE Transactions on*, vol. 15, pp. 1131-1147, 1993.

[4] C. Xu and J. L. Prince, "Snakes, shapes, and gradient vector flow," *Image Processing, IEEE Transactions on*, vol. 7, pp. 359-369, 1998.

[5] B. Li and S. T. Acton, "Vector field convolution for image segmentation using snakes," in *Image Processing, IEEE International Conference on*, Atlanta, GA, 2006.

[6] W. Neuenschwander, P. Fua, G. Szekely, and O. Kubler, "Velcro Surfaces: Fast Initialization of Deformable Models," *Computer Vision and Image Understanding*, vol. 65, pp. 237, 1997.

[7] R. Ardon and L. D. Cohen, "Fast Constrained Surface Extraction by Minimal Paths," *International Journal of Computer Vision*, vol. 69, pp. 127-136, 2006.

[8] T. McInerney and D. Terzopoulos, "Topology adaptive deformable surfaces for medical image volume segmentation," *Medical Imaging, IEEE Transactions on*, vol. 18, pp. 840-850, 1999.

[9] P. Perez, M. Gangnet, and A. Blake, "Poisson image editing," *ACM Transactions on Graphics (SIGGRAPH 03)*, vol. 22, pp. 313-318, 2003.

[10] S. T. Acton, "Multigrid anisotropic diffusion," *Image Processing, IEEE Transactions on*, vol. 7, pp. 280-291, 1998.

[11] Y. Yu and S. T. Acton, "Speckle reducing anisotropic diffusion," *Image Processing, IEEE Transactions on*, vol. 11, pp. 1260-1270, 2002.

[12] W. E. Lorensen and H. E. Cline, "Marching cubes: A high resolution 3D surface construction algorithm," *Computer Graphics*, vol. 21, pp. 163-169, 1987.

[13] A. V. Patil, C. D. Garson, and J. A. Hossack, "3D Prostate Elastography: Algorithm, simulations, and experiment," *Physics in Medicine and Biology*, submitted Dec. 2006.

Table 1. The computational complexity of different methods for solving a Poisson equation with N pixels.

SOR	CG	FFT	multigrid
$O(N^{1.5})$	$O(N^{1.5})$	$O(N \log N)$	$O(N)$

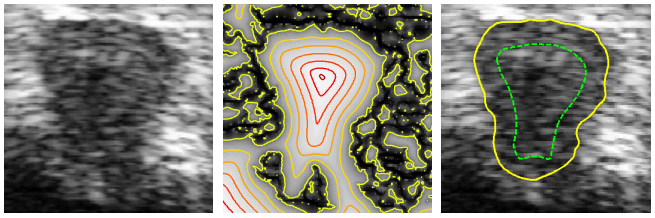

(a) (b) (c)

Fig. 1. (a)An ultrasound image of the prostate and (b) the PIG result of the VFC field overlapped with isolines. (c) The initial (green dashed line) and final (yellow solid line) snakes after 205 iterations using the PIG approach.

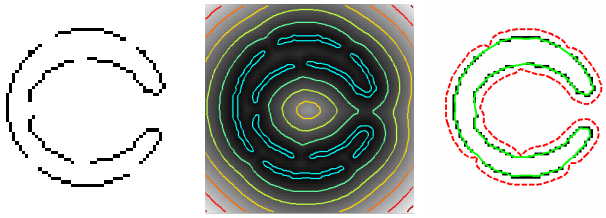

(a) (b) (c)

Fig. 2. (a) A synthetic broken c-shape edge. (b) The PIG result of the VFC field overlapped with isolines. (c) The initial (red dashed line) and final (green solid line) snakes after 12 iterations using the PIG initialization.

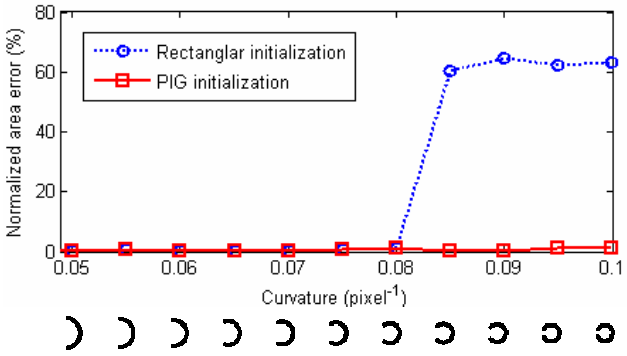

Fig. 3. The normalized area error using rectangular and PIG initializations for shapes with increasing curvature as shown below the plot.

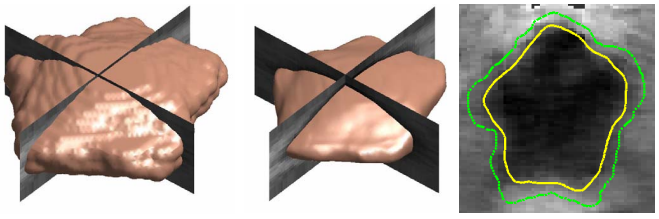

(a) (b) (c)

Fig. 4. (a) A 3D ultrasound image of simulated prostate lesion with the PIG initialization. (b) The VFC deformable surface deformed from the initial isosurface after 20 iterations. (c) The intersection of the middle image slices with the initial (green dashed lines) and final (yellow solid lines) VFC deformable surfaces.